USGS
science for a changing world

Geomagnetism Program

Prepared in cooperation with National Center for Atmospheric Research
High Altitude Observatory

Synthesizing Ground Magnetic Disturbance Using Dipole-Aligned Loop Elementary Currents and Biot-Savart Relationship

Scientific Investigations Report 2021–5123

U.S. Department of the Interior
U.S. Geological Survey

Synthesizing Ground Magnetic Disturbance Using Dipole-Aligned Loop Elementary Currents and Biot-Savart Relationship

By E. Joshua Rigler and Michael Wiltberger

Geomagnetism Program
Prepared in cooperation with National Center for Atmospheric Research
High Altitude Observatory

Scientific Investigations Report 2021–5123

U.S. Department of the Interior
U.S. Geological Survey

U.S. Geological Survey, Reston, Virginia: 2022

Suggested citation:
Rigler, E.J., and Wiltberger, M., 2022, Synthesizing ground magnetic disturbance using dipole-aligned loop elementary currents and Biot-Savart relationship: U.S. Geological Survey Scientific Investigations Report 2021–5123, 17 p., https://doi.org/10.3133/sir20215123.

ISSN 2328-0328 (online)

Acknowledgments

Michael Wiltberger was supported in part by the National Science Foundation Independent Research/Development Program. We thank Benjamin Murphy, Jeffrey Love, Kristen Lewis, and Brian Shiro from the U.S. Geological Survey for their helpful discussions and reviews.

Contents

Figures

Conversion Factors

International System of Units to U.S. customary units

Multiply	By	To obtain
	Length	
kilometer (km)	0.6214	mile (mi)

Abbreviations

3D	three dimensional
DALEC	dipole-aligned loop elementary current
DALECS	dipole-aligned loop elementary current system
DECS	dipolar elementary current system
FAC	field-aligned current
GGCM	global geospace circulation model
LFM	Lyon-Fedder-Mobarry
MHD	magnetohydrodynamic
MIX	magnetosphere-ionosphere cross coupler
SCHA	spherical cap harmonic analysis
SECS	spherical elementary current system
SHA	spherical harmonic analysis

Synthesizing Ground Magnetic Disturbance Using Dipole-Aligned Loop Elementary Currents and Biot-Savart Relationship

By E. Joshua Rigler[1] and Michael Wiltberger[2]

Abstract

This report presents a method for constructing a simplified numerical description of the electric current distributions in the ionosphere and gap region based on dipole-aligned loop elementary currents (DALECs). A theoretical basis for DALECs is presented, along with a prototypical algorithm for constructing an elementary numerical DALEC. The algorithm is verified and validated by combining DALECs with an efficient Biot-Savart solver in order to estimate magnetic disturbance on the Earth's surface. We examine (1) simple scenarios with known solutions and (2) hemispherical magnetic disturbance fields obtained from a state-of-the-art global geospace circulation model.

Introduction

The magnetic field measured on Earth's surface varies in intensity and orientation on different time scales. The longest scales, perhaps tens of months to millions of years, are associated with slow changes in the geodynamo that diffuse outward from the Earth's liquid iron outer core, through the mantle and crust, and finally into the geospace environment (Wardinski, 2007). The result is, at least presently, a multipolar geomagnetic field with a dominant dipole component that is roughly aligned with the Earth's rotational axis. This "main field" has been critical to terrestrial navigation for centuries, serves to dynamically organize the near-Earth space plasma environment for many research and operational applications, and is of little or no further interest to the rest of this discussion.

Shorter time scale variations in the geomagnetic field, perhaps fractions of a second to tens of years, are primarily the consequence of dynamical changes in ubiquitous electrical current distributions in the geospace environment (Constable, 2007). These include currents flowing in the more distant magnetosphere, the dynamical behavior of which is largely governed by magnetohydrodynamics (MHD). Other currents flow in the nearby ionosphere, where quasistatic electromagnetic assumptions often hold, so that variations in conductivity govern their spatial distribution. Currents flowing between these regions pass through a "gap" where the physics are less well understood, but currents are known to flow largely parallel to the magnetic field lines. These variations compose much of what has come to be referred to as "space weather" or "space climate" and include periodic magnetic tides (for example, Love and Rigler, 2014), as well as less regular variations that take the form of transient geomagnetic storms and substorms (Tsurutani and others, 1997).

More recently, the direct impact of geomagnetic perturbations on ground-based technological systems has come to be appreciated. For example, the modern oil and gas industry relies on accurate estimates of local magnetic declination for directional drilling. At high latitudes, large magnetic storms and substorms can force the needle of a compass several tens of degrees away from its nominal direction (Buchanan and others, 2013). These magnetic variations can also induce significant electric fields at the Earth's surface. This is a particular concern for high-voltage electric power distribution networks with nominally alternating current designs that can be compromised by the quasi-direct currents that result from the induced electric field. These direct currents can trigger network safeguards prematurely or, in extreme cases, damage or destroy multi-million-dollar transformers used to amplify comparatively low local voltages up to the hundreds of kilovolts needed to transmit power across long distances (Boteler, 2001; Love and others, 2014; Pulkkinen and others, 2017). These complicated networks operate very close to their capacity much of the time, which means that local complications can quickly cascade to neighboring sites, leading to systemic failure and large-scale blackouts. Accurate and timely magnetic measurements can be combined with knowledge of subsurface electrical conductivity to estimate the geoelectric fields over which the electric power distribution network operates.

An important challenge when mitigating such technological hazards is the sparse and uneven geographic distribution of magnetic observatories that are not generally located near infrastructure of interest. Interpolation can be used to address this issue, but naive two-dimensional interpolation based on nonphysical basis functions has been shown to perform poorly (for example, Xu and others, 2013; Rigler and others, 2019).

[1]U.S. Geological Survey.

[2]National Center for Atmospheric Research, High Altitude Observatory.

This is because the basis functions are poorly constrained far from actual measurements, which tends to amplify geospatial trends unrealistically. Optimal statistical interpolation (that is, Kriging) constrains the two-dimensional solutions reasonably well but is not amenable to physical interpretation or integration with physical models.

Physics-inspired basis functions can be fit to data and used to fill gaps between observed magnetic fields in a self-consistent manner. Spherical harmonic analysis (SHA; Chapman and Bartells, 1940) expands magnetic potential into a series of spherically periodic basis functions. Because SHA is poorly constrained by measurements that are not global in their distribution, spherical cap harmonic analysis (SCHA; Haines, 1985) expands magnetic potential within a "cap" that extends over only a part of a sphere and is used to calculate geomagnetic disturbance over a more localized region (for example, Haines, 1988; Haines and Torta, 1994; Weimer, 2005; Pothier and others, 2015; Waters and others, 2015; Fiori, 2020).

A comparable approach is to invert for equivalent ionospheric toroidal currents using a divergence-free spherical elementary current system (SECS; Amm, 1997), and from these estimate surface poloidal magnetic perturbations at arbitrary locations (for example, Amm and Viljanen, 1999; Pulkkinen and others, 2003b; McLay and Beggan, 2010; Wei and others, 2013; Rigler and others, 2019). Compared to SHA and SCHA, SECSs require the extra step of estimating magnetic fields from electric currents according to Maxwell's laws, but the SECS geometry exploits a simple analytic relationship to reduce the computational expense to something comparable to SHA and SCHA, while offering the extra benefit of an equivalent current distribution that can be useful in ionospheric studies (for example, Pulkkinen and others, 2003a; Weygand and others, 2011; Amm and others, 2015; Weygand and Wing, 2016; Marsal and others, 2017; Vanhamäki and Juusola, 2018). A thorough review of SECS can be found in Vanhamäki and Juusola (2020).

Fukushima (1976) explained how such current distributions might be adequate to explain all perturbations, but only if additional physical and geometric assumptions were made. Specifically, the magnetic signature from a radial line current will perfectly cancel that of the associated poloidal Pedersen current (with constant divergence) that must exist on a uniformly conducting sphere to maintain current continuity. This leaves only toroidal currents detectable on the ground. However, magnetic field lines are not in general radial nor are ionospheric conductances uniform, so the cancellation of the Pedersen currents is almost never perfect.

These violations to Fukushima's assumptions (1976) are often ignored with the argument that resulting ground magnetic disturbance is small (for example, Raeder and others, 2001). However, these discrepancies can be significant, up to several tens of nanoteslas. Moreover, to ignore magnetic field-aligned currents (FACs) and associated Pedersen currents is to ignore a primary source of energetic coupling between the ionosphere and magnetosphere. Indeed, most modern global geospace circulation models (GGCMs; for example, Lyon and others, 2004; Tóth and others, 2005; Raeder and others, 2013) include at least rudimentary ionospheric dynamics that rely on magnetic FACs. Relatively recently, with the validation and integration of GGCMs into space weather operations, some have found it prudent to include FACs in their calculations of geomagnetic disturbance (for example, Yu and others, 2010; Rastätter and others, 2014). This extends the range of model output validity beyond just the highest geomagnetic latitudes and allows practical predictions of geomagnetic disturbance over regions of the Earth's surface most at risk from space weather.

We propose a nuanced deviation from these latter GGCM studies based on a (magnetic) dipole-aligned loop elementary current system (DALECS). The concept of a dipole-aligned loop is not new, being first proposed by Boström (1964). In fact, Boström (1964) described two distinct electric current sheet loops: a Type 1 loop that flows zonally in a height-integrated spherical-shell ionosphere, in and out along dipole magnetic field lines with shared latitudinal bounds, and completes via a zonal equatorial current; and a Type 2 loop that flows meridionally, in and out along field lines with shared longitudinal bounds, and completes via a radial equatorial current (see fig. 1). These simple models were studied thoroughly through the 1960s and 1970s, combining ground magnetic measurements with some of the earliest computer simulations in space physics research (for example, Bonnevier and others, 1970; Kisabeth and Rostoker, 1977).

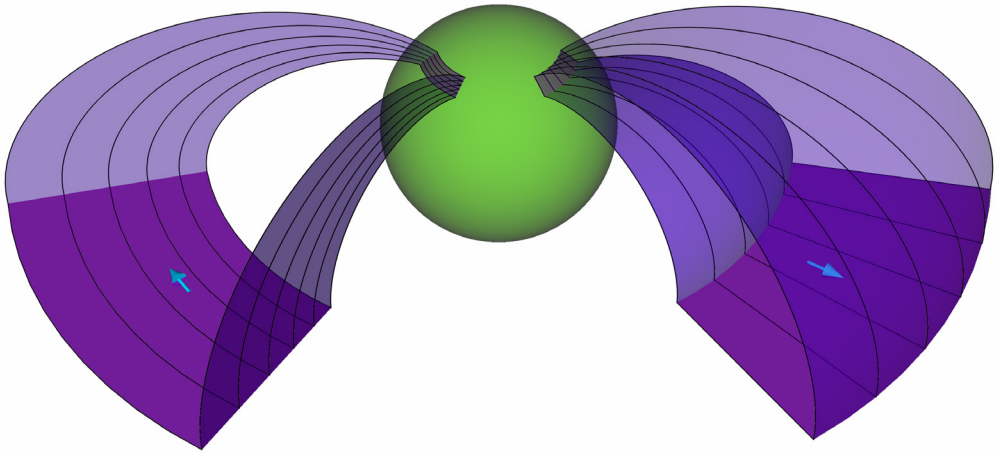

Figure 1. Image showing Boström's Type 1 (left) and Type 2 (right) current sheet loops.

Observational uncertainty and theoretical disagreements remain among space physicists concerning the detailed physics that might drive these electric current systems. See Kepko and others (2015) for an excellent historical perspective and summary of the present scientific consensus and Akasofu (2011) for an intriguing non-consensus viewpoint. However, there is general agreement that Type 1 loops represent the substorm current wedge (McPherron and others, 1973) and its associated westward ionospheric current, and Type 2 loops are responsible for auroral brightening via downward electron flow into the upper atmosphere. What we propose herein, however, is not a new physical interpretation of long-studied magneto-ionospheric phenomena and is certainly not a resolution to any long-standing debates in space physics. Rather, we use these well-established physical concepts to define a physics-motivated numerical basis for modeling the so-called gap region in magnetosphere-ionosphere coupling that can be easily used to calculate synthetic geomagnetic perturbations.

The remainder of this report details the physical and mathematical theory underlying DALECs, and offers a software algorithm to construct a self-consistent grid of elementary Type 1 and Type 2 current sheet loops that can be used to simulate ground magnetic disturbance when combined with the Biot-Savart law. For verification, we reproduce some of the early results of Boström (1964), Bonnevier and others (1970), and Kisabeth and Rostoker (1977). For validation, we combine a gridded system of DALECs with the Lyon-Fedder-Mobarry (LFM; Lyon and others, 2004) GGCM, using the magnetosphere-ionosphere cross coupler (MIX; Merkin and Lyon, 2010) to synthesize realistic magnetic perturbation distributions on Earth's surface, and demonstrate the value added when more realistic field line geometries are considered for equivalent current bases.

This work is consistent with U.S. Geological Survey Geomagnetism Program priorities (Love and others, 2020, Project 2), the priorities of the U.S. Geological Survey Natural Hazards Mission Area for improving hazard assessments (Holmes and others, 2013, Goal 3), and national priorities for enhancing space-weather modeling methods (National Science and Technology Council, 2019, Task 2.5).

Physics and Mathematical Theory

Bonnevier and others (1970) provided a mostly analytic solution to determine the magnetic perturbation caused by a combined Type 1-Type 2 Boström loop pair. However, their solution was not mathematically simple and still required limited numerical integration to obtain a useful solution to all but the simplest of loop configurations. We take a somewhat different approach that exploits the power and memory available in modern computer hardware and calculates a largely numerical solution. In short, we discretize a DALEC to an adequate spatial resolution, then use the Biot-Savart relationship to estimate magnetic perturbations at any point in space outside the loop. We review these well-established physical and mathematical theories before describing how they are combined algorithmically to produce a system of DALEC basis functions.

Magnetic Dipole Coordinates

Discretizing each Boström loop within a DALEC involves tracing dipole magnetic field lines. The required coordinate transformations can defy intuition and become computationally burdensome if not handled carefully. Fortunately, a magnetic dipole lends itself to constructing a right-handed orthogonal coordinate system with relatively straightforward analytic expressions to transform to/from standard spherical polar coordinates. This allows a simple loop to be constructed in magnetic dipole coordinates first, then transformed into more realistic spherical coordinates. Kageyama and others (2006) and Swisdak (2006) both summarize the relevant mathematics; we mostly follow the notation of Swisdak here:

$$q = \frac{\cos\theta}{\rho^2}, p = \frac{\rho}{\sin^2\theta}, \phi = \phi, \tag{1}$$

where

- ρ is the radius in spherical polar coordinates;
- θ is the co-latitude in spherical polar coordinates;
- ϕ is the longitude in both spherical polar coordinates and dipole coordinates;
- p parameterizes displacement perpendicular to a dipole field for constant, ϕ, and is therefore itself constant along a dipole field line; and
- q parameterizes displacement parallel to a field line such that $q = 0$ at the magnetic equator, $q \rightarrow -\infty$ as $\theta \rightarrow \pi$, and $q \rightarrow +\infty$ as $\theta \rightarrow 0$.

Using equation 1, a loop can be defined as a dipole axis-aligned rectangle. Converting the position of discrete segments of this rectangle into spherical coordinates requires inverting equation 1, which in turn involves the solution to a nontrivial equation. A computationally stable version of this inversion is:

$$\alpha = \frac{256}{27} q^2 p^4, \beta = \left(1 + \sqrt{1+\alpha}\right)^{2/3}, \gamma = \sqrt[3]{\alpha}, \tag{2}$$

$$\mu = \frac{1}{2}\left(\frac{\beta^2 + \beta\gamma + \gamma^2}{\beta}\right)^{3/2}, \text{ and} \tag{3}$$

$$\rho = \frac{4\mu}{(1+\mu)\left(1+\sqrt{2\mu-1}\right)} p, \theta = \sin^{-1}\left(\sqrt{\rho/p}\right), \phi = \phi, \tag{4}$$

where

- α is an intermediate value used to solve equation 1 for ρ and θ given p and q;
- β is an intermediate value used to solve equation 1 for ρ and θ given p and q;
- γ is an intermediate value used to solve equation 1 for ρ and θ given p and q; and
- μ is an intermediate value used to solve equation 1 for ρ and θ given p and q.

In addition to these positional transforms, discrete vector quantities constructed in dipole coordinates need to be converted to spherical coordinates. A directional vector component along a particular axis is the product of a scalar and unit vector associated with that axis. So, unit-vector transformations from dipole coordinates to spherical are required:

$$\delta = \sqrt{1 + 3\cos^2\theta}\,, \text{ and} \tag{5}$$

$$\hat{\boldsymbol{\rho}} = -\frac{2\cos\theta}{\delta}\hat{\mathbf{q}} + \frac{\sin\theta}{\delta}\hat{\mathbf{p}},\ \hat{\boldsymbol{\theta}} = -\frac{\sin\theta}{\delta}\hat{\mathbf{q}} - \frac{2\cos\theta}{\delta}\hat{\mathbf{p}},\ \hat{\boldsymbol{\phi}} = \hat{\boldsymbol{\phi}}, \tag{6}$$

where

δ is an intermediate value used to obtain unit vectors aligned with dipole axes; and

$\hat{\ }$ signifies a unit vector along the specified axis.

So, for example, if a segment of a Boström loop has an associated current vector only parallel to the magnetic field line (that is, along the q axis), in spherical coordinates it will have components in both polar angle θ and radial direction ρ. Furthermore, the transformation is dependent on the location of the vector, or at least on its polar angle.

Converting the length of a path between two points is often necessary. For arbitrary paths, this can be complicated, but if the path can be decomposed into segments parallel to each of the orthogonal magnetic dipole axes, there exist straightforward transformations into pathlengths in spherical coordinates:

$$dl_{\hat{\mathbf{q}}} = \frac{\rho^3}{\delta}\,dp, dl_{\hat{\mathbf{p}}} = \frac{sin^3\theta}{\delta}\,dp, dl_{\hat{\phi}} = \rho\sin\theta d\phi\,, \tag{7}$$

where

$dl_{\hat{\ }}$ is the pathlength parallel to unit vector converted to same units as ρ.

For the sake of completeness, we acknowledge that a Type 2 Boström loop is never a perfect rectangle in magnetic dipole coordinates and that its ionospheric segment follows a path along the ionospheric spherical shell with length $dl_{\hat{\theta}}=\rho d\theta$.

Dipole-Aligned Loop Elementary Current

Using the geometric relationships discussed in previous sections, one can construct a closed current loop basis composed of both a Type 1 and a Type 2 Boström loop. To start, assign a current sheet density vector with both meridional and zonal components at a single coordinate on a spherical shell. To convert the zonal component of this current sheet density into a current, assume it is meridionally uniform and multiply by its meridional extent, that is $dl_{\hat{\theta}}$. Likewise, to convert the meridional component of this current sheet density into current, assume it is zonally uniform and multiply by its zonal extent, that is $dl_{\hat{\phi}}$.

These currents will remain constant around their respective Type 1 and Type 2 loops, so it is now simple to construct a loop of current vector segments in magnetic dipole coordinates: just define nonoverlapping segments of the rectangle, assign the constant current to each segment (taking care to assign the correct sign), and calculate the length of the segment as the vector difference in neighboring magnetic dipole coordinates. If current densities of each segment are also required, it is necessary to calculate a cross section, but this is also straightforward in magnetic dipole coordinates. We now have a well-defined set of (1) magnetic dipole coordinates of discrete segments of the Type 1 and Type 2 Boström loops; (2) an associated directional vector for each segment, scaled by the constant current; and (3) a length and cross section for each segment, all in magnetic dipole coordinates. All that remains is to transform these back into spherical coordinates using equations 2–7.

Biot-Savart Relationship

The Biot-Savart relationship is an empirical relationship that describes the magnetic field generated by an electric current that is constant in time (that is, the magnetostatic approximation). It is named after Jean-Baptiste Biot and Felix Savart, who discovered the relationship in 1820. It is consistent with Ampere's original circuital law but without Maxwell's displacement current correction. It predates Maxwell's more complete electromagnetism equations by about 40 years. The Biot-Savart relationship is

$$\mathbf{B} = \frac{\mu_0}{4\pi}\iiint_V \frac{\mathbf{J}dV\times(\mathbf{r}-\mathbf{r}')}{|\mathbf{r}-\mathbf{r}'|^3}\,, \tag{8}$$

where

$\mathbf{r}$ is the three-dimensional location of magnetic field estimate;

$\mathbf{r}'$ is the three-dimensional location of differential current density element;

$\mathbf{B}$ is the magnetic field vector at $\mathbf{r}$;

μ_0 is the magnetic permeability of free space;

$\mathbf{J}$ is the differential current density vector at $\mathbf{r}'$; and

dV is the differential volume/area/length associated with $\mathbf{J}$ at $\mathbf{r}'$.

Essentially, equation 8 formalizes the right-hand rule of thumb so often invoked to crudely describe magnetic field lines (represented by curled fingers) generated by a line current segment (represented by the thumb). It is actually an indirect solution to Ampere's law ($\nabla\times\mathrm{B}=\mu_0\,\mathbf{J}$), whereby some helpful vector identities have been applied to the curl of the magnetic vector potential ($\nabla\times\mu_0/4\pi\iiint_V \mathbf{J}dV/|\mathbf{r}-\mathbf{r}'|^3$) to provide a mathematically simplified relationship that could be implemented efficiently as a computer algorithm. This is important because, if the current density distribution is not analytically

integrable, it will need to be discretized such that associated error is minimized for numerical integration. For most realistic scenarios, this requires a large number of discrete elements to be calculated and summed, so it is advantageous to implement an efficient algorithm.

Algorithms and Practical Considerations

A number of implementation details are left to the software designer, but the pseudocode presented in appendix 1 captures the most pertinent aspects of a Python module used to verify and validate the DALEC concept in the Verification and Validation section. With the noted exception of array operations, the algorithms are presented as linear procedures for the sake of algorithmic clarity. Undoubtedly, there are design choices available that could improve performance significantly.

At first glance, algorithms 1 and 2 in appendix 1 may appear to be largely similar; indeed, the numerous redundancies can be exploited to further improve performance. However, there are also key differences that users must not ignore. Their inputs are almost identical, except for the current sheet density of the input ionospheric segment (J_ϕ for Type 1 and J_θ for Type 2 loops). As for outputs, there are $2N$+2 current sheet segments (N is chosen by the user) for each position vector ($\mathbf{r}_{out} \in \mathbb{R}^3$), current density vector ($\mathbf{J}_{out} \in \mathbb{R}^3$), and scaling factors ($\mathbf{l}_{out} \in \mathbb{R}^2$). For the Type 1 loop, these comprise N segments for each of an inward and outward FAC along dipolar magnetic field lines that are identical in all but their longitudes, plus a longitudinal current sheet density for the ionosphere, and a longitudinal current sheet density in the equatorial plane. Likewise, the Type 2 loop is broken into $2N$+2 segments, but the inward and outward FACs flow along different dipolar magnetic field lines with identical longitudes, the ionospheric segment current sheet density is latitudinal, and the equatorial segment current sheet density is radial. The ionospheric segments are identical to the inputs J_ϕ and J_θ.

With a complete two-loop DALEC constructed in spherical coordinates, the Biot-Savart relationship can be used to estimate its magnetic influence at any point on Earth's surface. Although the Biot-Savart integral can certainly be represented in spherical coordinates (for example, Kisabeth and Rostoker [1977]), it has been our experience that it is more computationally efficient to implement it in Cartesian coordinates and then to use optimized mathematical libraries to convert from, and back to, spherical coordinates as needed. This Cartesian Biot-Savart integration is represented in algorithm 3 in appendix 1 using a standard for-loop mechanism to make the summation obvious. This process could easily be implemented using matrix multiplication in many modern mathematical libraries, which is likely to be much faster than using a standard for-loop mechanism.

Thus far, we have described basic algorithms for generating a single (two-loop) DALEC (uniquely characterized by its latitudinal and longitudinal ionospheric sheet current density) along with the geographic radius, width, and length of this ionospheric sheet segment. From these calculations, it is possible to estimate the magnetic perturbation that would be produced at any point outside the DALEC's three-dimensional (3D) boundaries. If we were to generate a second DALEC with a sheet current that aligned with one of the sheet currents of the first DALEC, the difference in their coincident FACs would equal the discrete divergence of the ionospheric segments. Finally, if we were to generate a regular grid of such aligned DALECs, it could faithfully represent the ionospheric current sheet density distribution expected from a physically self-consistent, if simplified, height-integrated ionosphere.

There will likely be noticeable discretization artifacts if the distance between a DALEC element and a point at which a magnetic perturbation estimate is desired is comparable to, or less than, the spacing between the discrete DALEC elements themselves. This is a common problem when the perturbation estimate is desired on Earth's surface because the ionosphere's altitude is roughly 100 kilometers, and grid spacing for the ionospheric segments is typically larger than this. If this is unacceptable for the intended application, a simple numerical approach may suffice: near those locations where synthetic measurements are desired, users can simply subdivide the original ionospheric segment into a grid of identical current density segments that only differ in their respective boundaries. We will refer to this collection of smaller DALECs as a "macro-" DALEC. The FACs internal to this macro-DALEC will cancel each other, but the sheet currents at the edges, especially the ionospheric sheet current, will now be discretized finely enough that the numerical artifacts should effectively disappear.

This numerical trick could easily become computationally intractable, or at least so slow as to discourage its use. However, a subtle aspect of the Biot-Savart relationship can be exploited to immensely accelerate calculations, at least after some otherwise computationally expensive precalculations are done, so long as the target locations for magnetic perturbation estimates do not change with respect to the DALEC. In this scenario, returning to equation 8, everything inside the Biot-Savart integral, except for the current density **J**, should be constant and, therefore, need only be calculated once before cross multiplying by the changing **J** values to generate a changing magnetic disturbance **B**. In algorithm 3 of appendix 1, this amounts to pre-calculating the dX, dY, dZ, dR, and dR^3 terms for all sheet current segments, then recalling these static values at each time step to combine with a new distribution of current density vectors.

Furthermore, if one recognizes that all currents inside a DALEC are proportional to (that is, scale linearly with) the input ionospheric current density, it should be clear that the magnetic field perturbation obtained from Biot-Savart must also scale linearly with the input ionospheric current density. Therefore, one may simply set the input ionospheric current

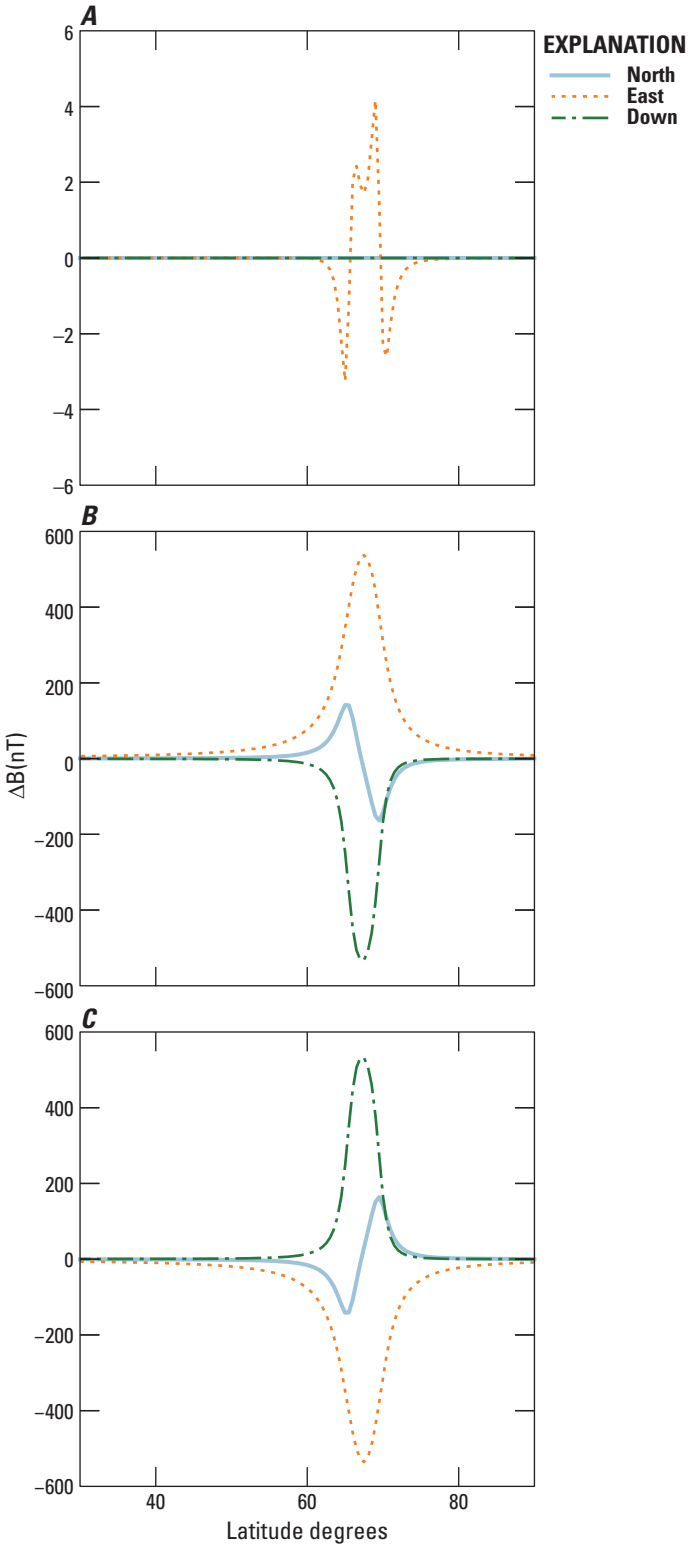

Figure 2. Graphs showing *A*, meridional transect of ground magnetic response to Type 2 Boström loop toroid constructed from dipole-aligned loop elementary currents; *B*, ground magnetic response to zonally bounded segment of Type 2 toroid measured at its eastern edge; and *C*, ground magnetic response to inverse of zonally bounded segment in figure 2*B*, measured at its western edge. (ΔB[nT], magnetic disturbance in nanoteslas)

densities J_θ and J_ϕ to unity, generate the corresponding DALEC, and then calculate the resulting magnetic perturbation at a desired location. After that, the magnetic field may be reestimated for arbitrary densities J_θ and J_ϕ simply by scaling the magnetic field obtained in the precalculation, where densities J_θ and J_ϕ were set equal to unity. This amounts to multivariate linear regression, and although users must be careful to ensure that the relative positions of the desired magnetic field output and the input DALEC current density segments do not change, it can accelerate the Biot-Savart estimation of magnetic field perturbations by several orders of magnitude, at least when using optimized modern linear algebra software libraries.

In short, not only can we synthesize a macro-DALEC to arbitrary numerical precision by building it from smaller elementary DALECs, but we can also construct a global grid of elementary DALECs to self-consistently represent horizontal ionospheric currents, FACs, and equatorial current sheets. This is still an equivalent current system and not a representation of the true magnetosphere-ionosphere system, but it is much closer to reality than the purely toroidal ionospheric current systems mentioned earlier and matches perfectly the geometric and physical assumptions implicit to many GGCMs.

Finally, it must be acknowledged that both Type 1 and 2 Boström loops are undefined if one of the FACs falls on a pole where p, and ultimately, FAC pathlengths become infinite. Technically, Type 1 loops are still defined at the equator, where q and FAC pathlengths are zero, but the longitudinal ionospheric and equatorial segments coincide and simply cancel each other out, so there is little reason to perform such calculations. Type 2 loops are valid when one FAC falls on the equator, because that only means the FAC has zero length, and therefore generates no magnetic disturbance. However, allowing the Type 2 loop to traverse the equator is problematic because, although the equations contain no infinities, this is no longer a closed current loop and, therefore, not "physical." Other well-defined, non-DALEC equivalent current systems could be specified at the pole or equator (for example, an equatorial ring current or an infinite polar radial current), but these fall outside the scope of this report and will not be discussed further.

Verification and Validation

Is it Correct?

Generally, verifying that an algorithm does what it is designed to do, correctly, is a worthwhile exercise. Because ours is a numerical implementation of a nominally physical system, this can be accomplished by reproducing certain analytic solutions. Bonnevier and others (1970) walk through a complicated derivation of an expression for magnetic perturbation from what amounts to a differential DALEC. Indeed, this method might even be preferred to our brute force

numerical approach except for its mathematical complexity and the fact that, in the end, a certain amount of numerical integration is still required for all but the simplest DALEC configurations. As it happens, the only fully analytic solution Bonnevier and others (1970) offer leads to zero magnetic perturbation everywhere outside the DALEC. Briefly, if the ionospheric segment current is uniform, only in the north-south orientation, and extends 360 degrees so that it closes on itself, a Type 2 Boström loop toroid results. By Ampere's law, any toroid is effectively an infinite solenoid and so produces zero magnetic field outside its current loops.

Figure 2*A* presents ground magnetic disturbance along a meridional transect that runs beneath a Type 2 Boström loop toroid with an integrated current of 90×10^6 amperes. The ionospheric segment of this toroid spans 65.5–69.5 degrees latitude before diverting current along the magnetic field lines. The y-axis scale in figure 2*A* is designed to make numerical artifacts from our chosen level of discretization (1 degree longitude by 0.2 degrees latitude, or roughly 42×22 kilometers at these latitudes) obvious, but the deviation from expected zero disturbance is less than 1 percent of the maximum disturbance obtained from a smaller toroid segment with identical current densities. Furthermore, we found that decreasing the size of the DALECs (that is, increasing the grid resolution) resulted in a systematic reduction of this deviation that appeared to converge on zero. The unrealistic integrated current used for figure 2*A* was chosen so that its density matched the somewhat more realistic Type 2 Boström loop toroid segment used to generate the magnetic disturbance in figure 2*B*, which has an integrated current of 1×10^6 amperes distributed evenly across 4 degrees longitude. Finally, figure 2*C* presents the magnetic disturbance generated by a toroid segment that spans the entire longitudinal range except the segment used to generate the geomagnetic disturbance presented in figure 2*B*. Figure 2*C* is a near-perfect reflection of the magnetic profile in figure 2*B*, which only makes sense if the two combine to equal zero disturbance, as expected.

Turning to Kisabeth and Rostoker (1977) for ideas to further test our DALECS algorithm, we constructed a Type 1 Boström loop spanning 0–20 degrees longitude and 65–70 degrees latitude with an integrated current of 1×10^6 amperes flowing westward in the ionosphere. No analytic solution for the magnetic disturbance caused by this analog of a substorm current wedge exists, but we can compare our results with those obtained by the original authors. Figure 3 presents contours of magnetic disturbance for each of three spherical coordinates, modified slightly from traditional spherical coordinates to match Kisabeth and Rostoker's presentation (1977).

The results are antisymmetric (eastward) or symmetric (northward and downward) about 10 degrees longitude, which is the center of this zonal loop, so we drop the redundant western half of the magnetic disturbance distribution. The lack of symmetry in the north-south orientation is due entirely to the dipole nature of the magnetic field lines. The overall shape and intensity of these contours match those of Kisabeth and Rostoker (1977) well. Slight discrepancies exist, but these are not unexpected if the current system discretization, or spatial sampling frequency of the estimated magnetic field, differ.

A similar comparison can be performed for a Type 2 Boström loop. In fact, the loop used to generate the results presented in figure 2*B* is the same loop studied by Kisabeth and Rostoker (1977). Figure 4 presents contours of magnetic disturbance for each of the same three spherical coordinates as before. Once again, the results are antisymmetric or symmetric about the zonal center of the current system, but this time the antisymmetry is in the northward magnetic disturbance. The results are not symmetric in the north-south orientation, and the overall shape and intensity of the contours match those of Kisabeth and Rostoker (1977) well, with slight discrepancies that result from different discretization schemes.

Is it Useful?

Having verified that our algorithm produces expected results to an accuracy limited only by the resolution of our discretization, the question remains: is our algorithm useful or, more importantly, is it reasonable to use it instead of simpler and less computationally expensive algorithms? We chose to validate the DALECs algorithm by combining it with LFM-MIX for the purpose of estimating ground magnetic disturbance caused by its current distributions. Briefly, this complicated magnetosphere-ionosphere model works as follows: given ionospheric Pedersen and Hall conductances generated empirically from FACs produced at the LFM model's inner boundary, MIX solves the current continuity equation, then uses the calculated ionospheric electric potential as part of a low-altitude boundary condition for the LFM model's MHD solution. This mostly self-consistent framework couples two physical modeling regimes with very different spatial and time scales, relying on a relatively simple geometric (dipole-field) mapping of the MHD inner boundary to ionospheric altitudes.

The LFM model does not output electric currents directly because they are not required for its MHD solution. (For the purposes of this study, MHD magnetospheric currents are not necessary, but for completeness, we note that these can be readily calculated from the curl of the local MHD magnetic field.) MIX does provide FAC densities that are mapped to the ionosphere; however, these are reproduced numerically by the divergence between neighboring DALECs, so we only use the MIX FACs for verification. As already noted, MIX also provides electric potential and conductance (Pedersen and Hall) distributions on a spherical ionosphere surface. When combined with Ohm's law, these electric conditions enable a straightforward calculation of the horizontal ionospheric sheet current densities, which in turn constitute the ionospheric segments of a system of DALECs.

These horizontal current sheets are presented as two-dimensional projections onto the northern hemisphere of a spherical ionosphere in figure 5. This snapshot in time was taken at 08:00 coordinated universal time from a simulation

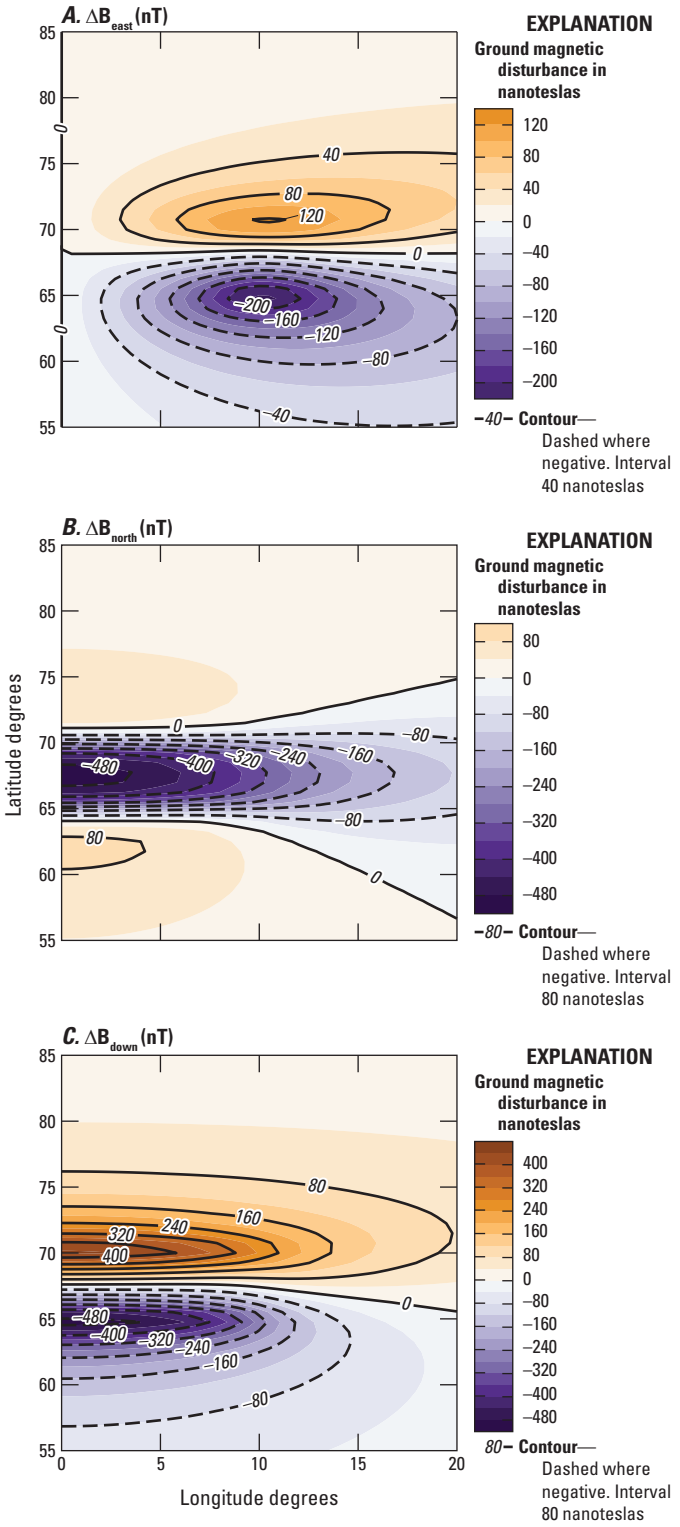

Figure 3. Graphs showing *A*, contours of eastward component of magnetic disturbance caused by a Type 1 Boström current sheet loop constructed to emulate a substorm current wedge; *B*, the northward component of magnetic disturbance caused by this Type 1 Boström loop; and *C*, the downward component of magnetic disturbance caused by this Type 1 Boström loop. (ΔB[nT], magnetic disturbance in nanoteslas)

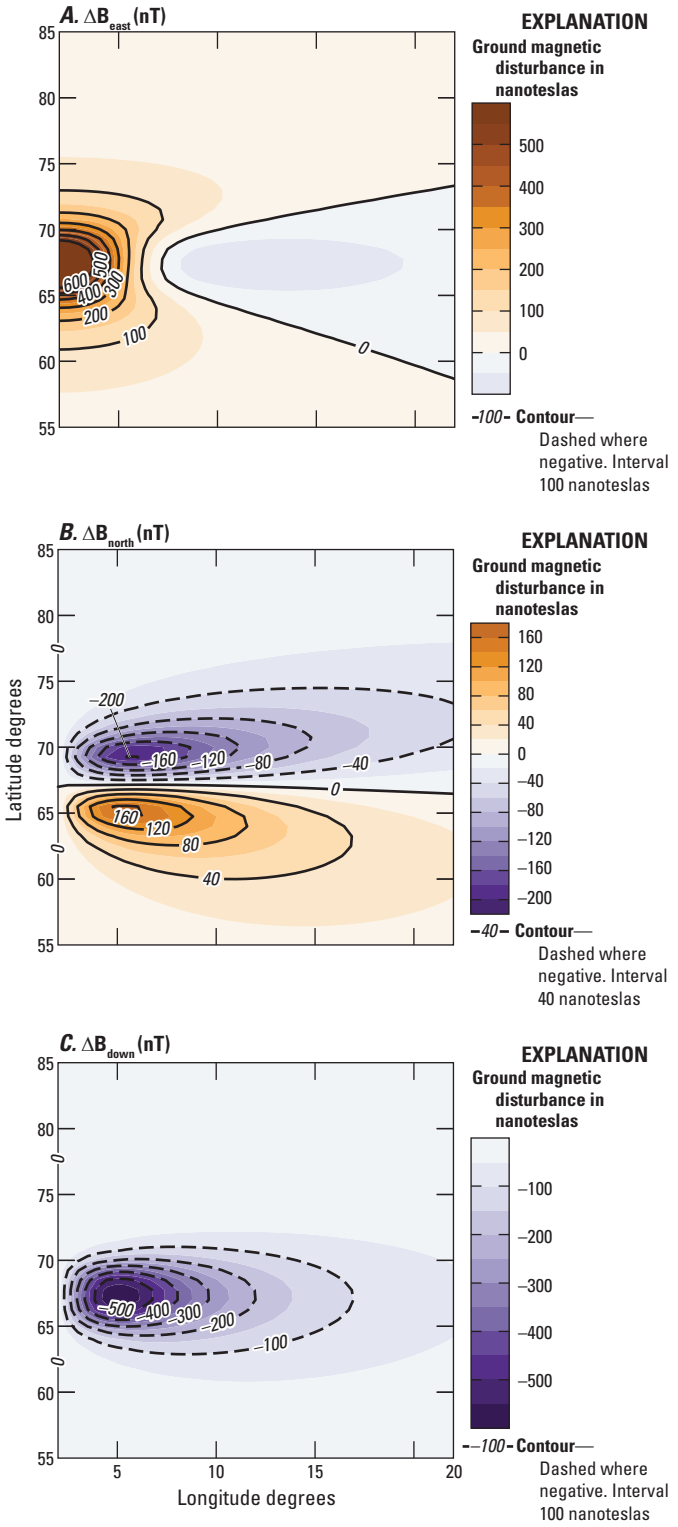

Figure 4. Graphs showing *A*, contours of eastward component of magnetic disturbance caused by a Type 2 Boström current sheet loop with a 4×4-degree ionosphere segment centered at +67.5 degrees latitude; *B*, northward component of magnetic disturbance caused by this Type 2 Boström loop; and *C*, downward component of magnetic disturbance caused by this Type 2 Boström loop. (ΔB[nT], magnetic disturbance in nanoteslas)

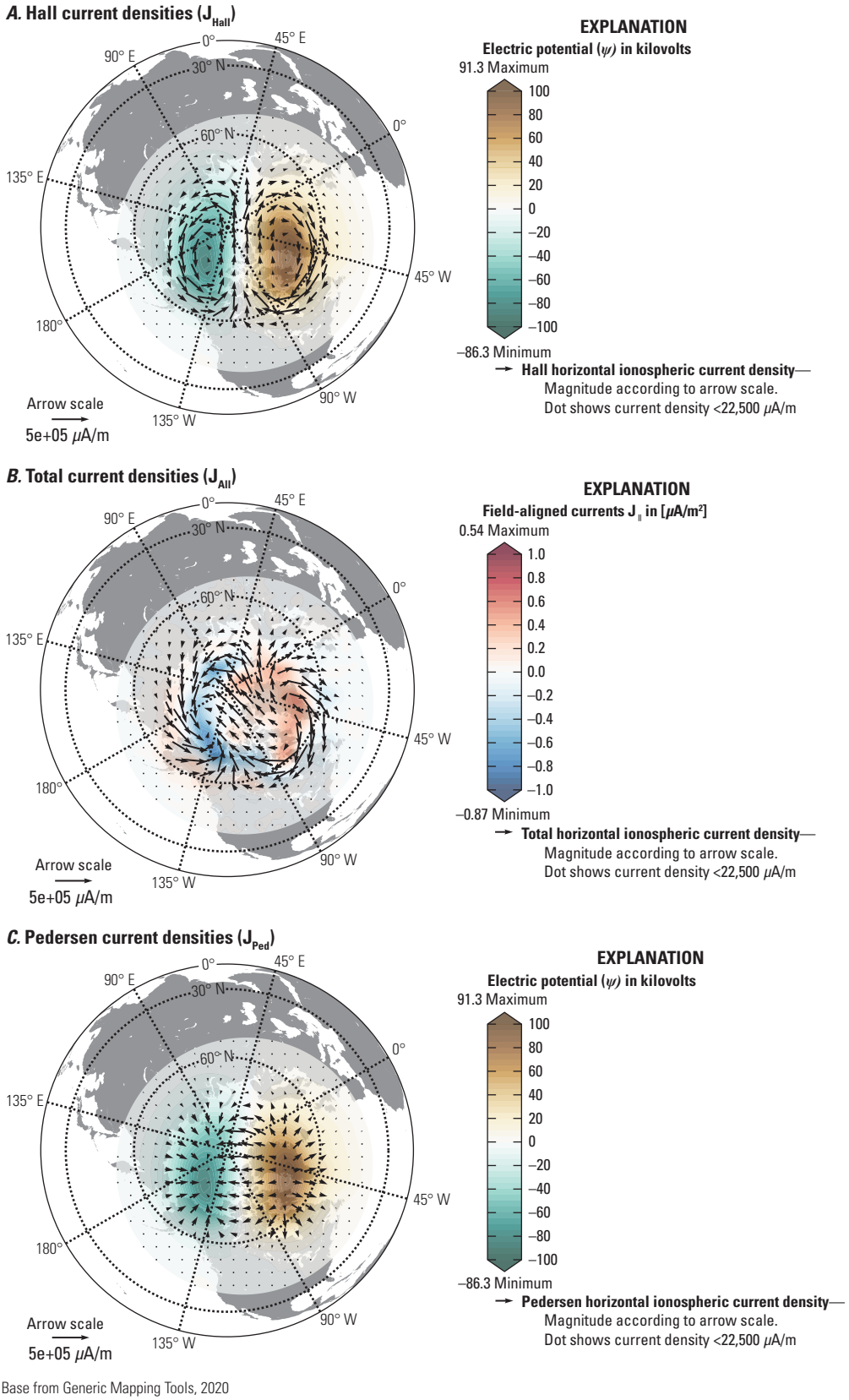

Figure 5. Maps showing *A*, electric potential (colored contours) and Hall horizontal ionospheric currents (arrows) from the Lyon-Fedder-Mobarry–magnetosphere-ionosphere cross coupler (LFM-MIX) global geospace circulation model (GGCM); *B*, field-aligned currents (colored contours) and total (Pedersen and Hall) horizontal ionospheric currents (arrows); and *C*, electric potential (colored contours) and Pedersen horizontal ionospheric currents (arrows). (μA/m, microamperes per meter; μA/m^2, microamperes per square meter)

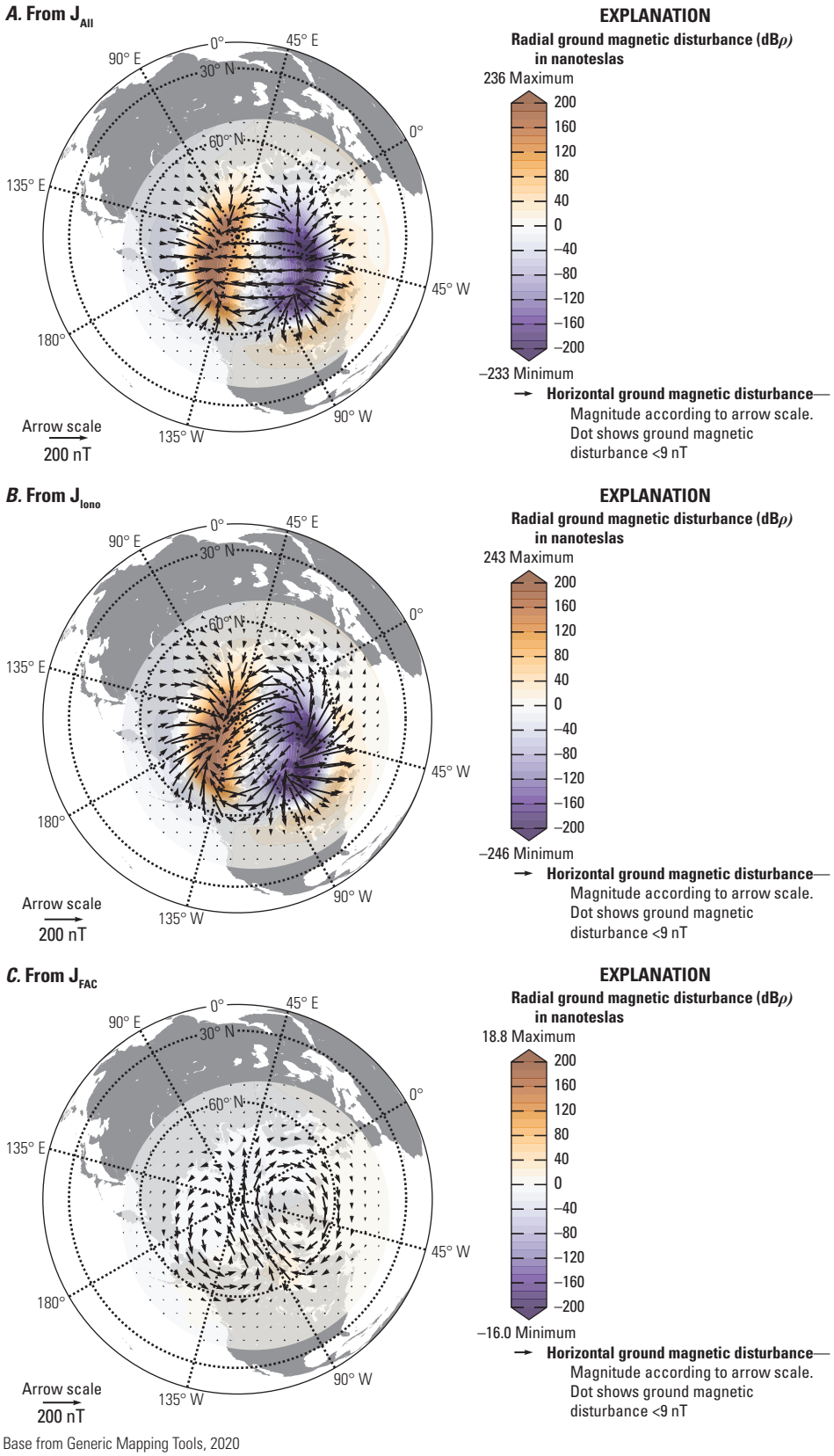

Figure 6. Maps showing *A*, vertical ground magnetic disturbance (colored contours) and horizontal ground magnetic disturbance (arrows) due to full dipole-aligned loop elementary currents (DALECs); *B*, vertical ground magnetic disturbance (colored contours) and horizontal magnetic disturbance (arrows) due to DALECs ionospheric segments; and *C*, vertical ground magnetic disturbance (colored contours) and horizontal magnetic disturbance (arrows) due to DALECs field-aligned current (FAC) and equatorial current segments. (nT, nanoteslas)

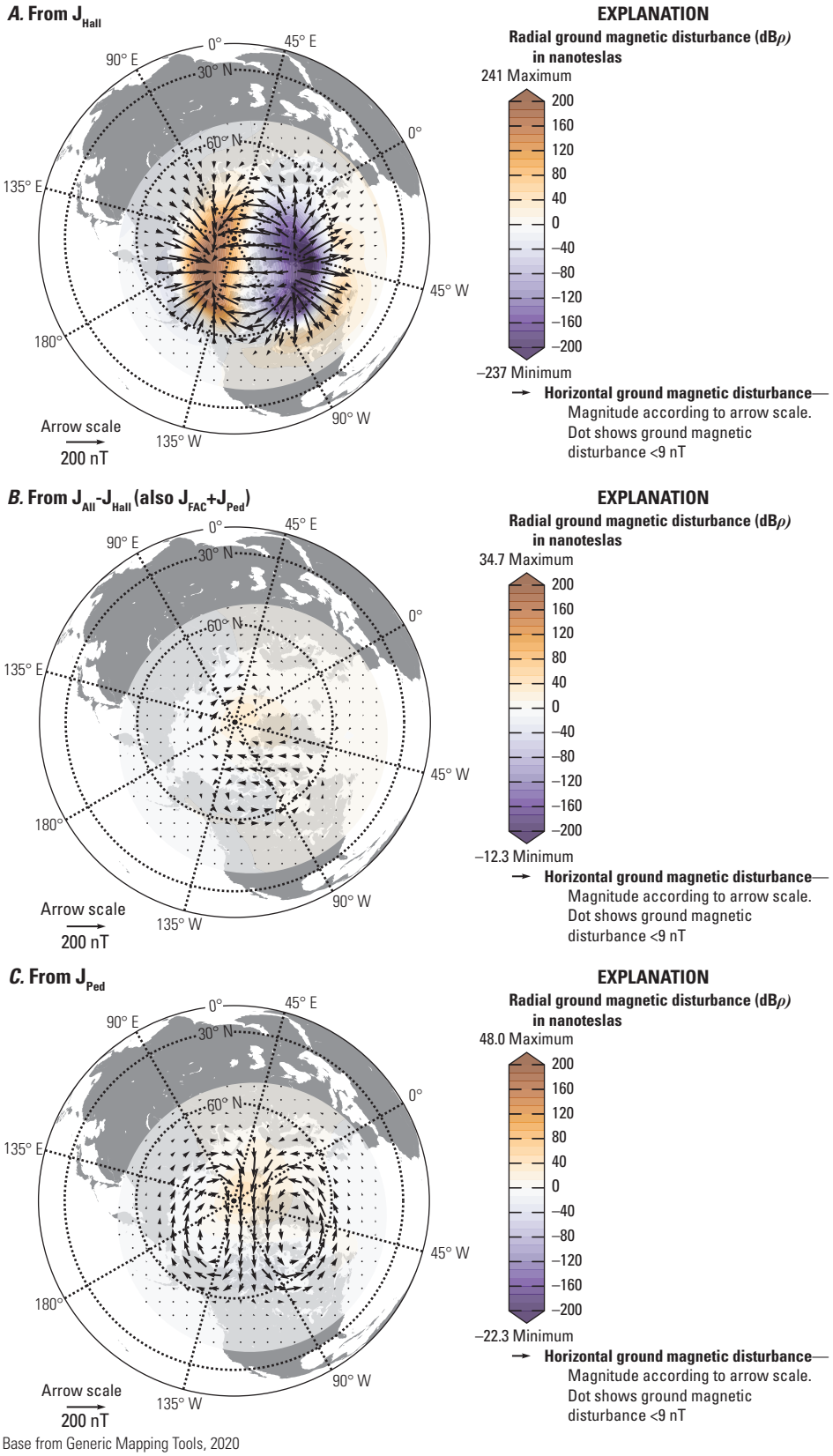

Figure 7. Maps showing *A*, vertical ground magnetic disturbance (colored contours) and horizontal magnetic disturbance (arrows) due to Hall currents; *B*, discrepancy in vertical ground magnetic disturbance (colored contours) and horizontal magnetic disturbance (arrows) (that is, all Hall or Pedersen [Ped] and field-aligned currents [FACs]); and *C*, vertical ground magnetic disturbance (colored contours) and horizontal magnetic disturbance (arrows) due to Pedersen currents. (nT, nanoteslas)

of a moderate geomagnetic storm that occurred on March 26, 2008. Because LFM-MIX provides both Pedersen and Hall conductances, current densities can be decomposed into Pedersen and Hall components. These are overlaid on the original potential field in figure 5*A* (Hall) and figure 5*C* (Pedersen). As expected, Pedersen currents flow in the direction of the electric field, which, for our magnetostatic approximation, is the gradient of the potential field. Hall currents flow parallel to contours of electric potential. Although the potentials and conductances used to generate these currents are obtained from a GGCM that models the entire magnetosphere, from this point forward, we assume that these currents exist in isolation and ignore any MHD magnetospheric currents that might exist. With a distribution of horizontal ionospheric current densities, a DALEC can now be constructed that self-consistently models 3D currents. FACs arise from the numerical divergence of the horizontal current sheet densities. When integrated across an ionospheric grid cell to give volume currents, these FACs match the FACs output by MIX to near-numerical precision. The FACs are shown in figure 5*B* as color contours, overlaid by the summation of Pedersen and Hall horizontal current densities.

The geomagnetic disturbance caused by the same 3D DALEC distribution summarized by figure 5 is presented in figure 6. Figure 6*A* shows the disturbance caused by all currents combined (that is, figure 5*B*). Figure 6*B* and 6*C* separate this into the components of disturbance caused by horizontal ionospheric currents and those caused by FACs, respectively. It is notable that the horizontal disturbance field in figure 6*A* roughly resembles what one would expect from the Hall currents in figure 5, although the horizontal disturbance field in figure 6*C* resembles what one would expect from a reversal of the Pedersen currents, if perhaps somewhat offset and rotated relative to the Pedersen currents in figure 5. However, these resemblances are far from perfect, and the discrepancies are made evident in figure 7, where figure 7*A* presents magnetic disturbance from the actual Hall currents alone and figure 7*C* presents magnetic disturbance from the actual Pedersen currents alone. Figure 7*B* shows the difference between the total current and Hall current disturbances, and it is also exactly the sum of the FAC and Pedersen current geomagnetic disturbances.

In short, figure 7*B* shows the discrepancy between a realistic geomagnetic signature—one that accounts for both nonradial FACs and nonuniform ionospheric conductances—and the signature that would be expected if all of Fukushima's assumptions were valid. It is this discrepancy that motivates our use of a system of DALECs, rather than simpler analytic expressions that rely on satisfying Fukushima's assumptions. The impact of nonradial FACs is relatively easy to understand and might even be amenable to a relatively simple correction, as Fukushima himself pointed out in his 1976 paper. However, even if magnetic fields were radial, realistic nonuniform conductances would lead to Pedersen currents that do not cancel the magnetic effects of radial FACs on the ground. In other words, equivalent Hall currents can never fully explain ground magnetic disturbance caused by a realistic 3D current distribution.

This is not to say that some other divergence-free equivalent current distribution could not reproduce an observed geomagnetic disturbance pattern—we already know this is possible from Amm and Viljanen (1999). However, any such distribution will not represent the true horizontal current distribution, especially at lower latitudes. Whether all this is of practical concern is, of course, a subjective matter, but we note that our simulation uses a relatively coarse grid and empirical estimates of conductance that tend to smooth this spatial distribution even further. More realistic conductance distributions are likely to exhibit much less uniformity and will therefore make it even less valid to assume that the geomagnetic disturbance caused by Pedersen currents and FACs cancel.

Broader Context and Future Work

This report presented a theoretical basis for a magnetic dipole-aligned loop elementary current (DALEC) system. A single DALEC (consisting of a Type 1 and Type 2 Boström current loop pair) is not especially novel, as numerical implementations of this three-dimensional electric current system were used to model substorms as early as the 1960s. The novel contribution here was our construction of a regular grid of DALECs with coincident dipolar FAC elements that can effectively reproduce the divergence of electric current in the ionosphere in a physically consistent and numerically structured manner.

We also presented a template algorithm and verified that a DALEC system does indeed reproduce many expected theoretical results by implementing this algorithm in the Python programming language. We demonstrated how such a system can be integrated with the LFM-MIX GGCM to simulate FACs and horizontal ionospheric currents, thus allowing ground magnetic perturbations to be accurately estimated using the Biot-Savart relationship. The latter may, at first, seem unnecessarily redundant to those not familiar with GGCMs. However, because magnetohydrodynamic models do not generally track current density as a state variable (current continuity is assumed) and require only ionospheric electric potentials to establish their inner boundary conditions, they have no explicitly calculated currents.

Our DALECS algorithm Python implementation has been included with the LFM-MIX software package and has been used in studies that compare and assimilate ground magnetic observations with simulated geospace current systems. However, we note that our algorithm is very flexible and is only loosely coupled with the LFM-MIX GGCM codebase. It can easily incorporate output from any model capable of producing horizontally integrated ionospheric current sheet distributions (most do this) and, combined with a Biot-Savart integrator, can synthesize magnetic disturbance on Earth's surface.

Recall from the Introduction section that much recent geomagnetism research has focused on the estimation of the geoelectric fields that drive geomagnetically induced currents in electrically conductive technological infrastructure. Although a gold standard toward this end might be to physically model the full electromagnetic response within the Earth to changes in geospace source currents (for example, Kelbert and others, 2014), this is, at present, not computationally feasible on a global scale or on any temporal scale other than short intervals. Until such physical modeling does become feasible, magnetotelluric impedances can simplify the estimation of geoelectric fields given geomagnetic disturbance fields as input. The problem with this, however, is that magnetotelluric impedances are generally obtained from ground-level magnetic measurements, which are a magnetic superposition of the effects of geospace source currents and induced telluric currents. To our knowledge, no GGCM to date accounts for the effects of induced currents in their estimates of geomagnetic disturbance.

A relatively simple solution that should improve simulated geomagnetic disturbance, to zeroth order at least, is to assume a super-conducting sphere below Earth's surface, thus allowing the use of so-called image dipoles. This was proposed and implemented by Kisabeth and Rostoker (1977). It was not implemented for the present study because our initial impression was that it would be too computationally expensive for real-time applications or global long-term analyses. However, this decision is worth reconsidering in light of some of the efficiencies noted previously in this report. In particular, under a quasi-static assumption, geomagnetic disturbance from a Type 1 or Type 2 current sheet loop of any intensity is merely a linear scaling of the disturbance estimated from similar Type 1 or Type 2 current sheets with a unit current sheet density in the ionosphere. The first round of computations may well be computationally expensive, but subsequent passes can be accelerated immensely using a simple linear regression.

Finally, to expand on this idea of linear regression, an empirical system of DALECs may easily be obtained by inversion of observed ground magnetic perturbations. This can be done in much the same way that Amm and Viljanen (1999) did with SECS (that is, scale the magnetic perturbations obtained from unit-amplitude current densities and transformed into a common coordinate frame). However, in our case, the horizontal ionospheric components are fitted for each DALEC. There is a potential problem with the lack of uniqueness apparent in figure 2*B–C*. However, mathematical uniqueness is not required to be practically useful in most geophysical applications, and there are ways the inversion problem can be constructed, constrained, and (or) regularized in its solution that can help mitigate this issue.

Recently, Vanhamäki and others (2020) published a similar, but not identical, technique that addresses the problem of nonradial FACs using curl-free horizontal ionospheric current distributions that close through interhemispheric dipolar FACs and connect areas designated as a "source" and "sink" at latitudinally symmetric locations. Their dipolar elementary current system (DECS) has at least one advantage over our DALECS in that it employs an analytic solution for magnetic disturbance from the ionospheric currents. However, like DALECs, the magnetic influence of FACs must still be estimated numerically using the Biot-Savart relationship. Unlike DALECs, DECs do not allow separation of the northern and southern hemispheres, nor do they model equatorial currents. DECs and DALECs have unique advantages and drawbacks in different situations, but both provide a more complete model of magnetosphere-ionosphere coupling than any other empirical methods presently in wide use. Therefore, both DECs and DALECs should improve interpolation between geographically sparse geomagnetic measurements, especially in mid-latitude regions with higher population densities that are most at risk for geomagnetic disturbance hazards.

References Cited

Akasofu, S.-I., 2011, The choice of the concept of magnetic field lines or of electric current lines—Alfvén medal lecture: Annales Geophysicae, v. 29, no. 7, p. 1215–1232.

Amm, O., 1997, Ionospheric elementary current systems in spherical coordinates and their application: Journal of Geomagnetism and Geoelectricity, v. 49, no. 7, p. 947–955.

Amm, O., Vanhamäki, H., Kauristie, K., Stolle, C., Christiansen, F., Haagmans, R., Masson, A., Taylor, M.G.G.T., Floberghagen, R., and Escoubet, C.P., 2015, A method to derive maps of ionospheric conductances, currents, and convection from the Swarm multisatellite mission: Journal of Geophysical Research, Space Physics, v. 120, no. 4, p. 3263–3282.

Amm, O., and Viljanen, A., 1999, Ionospheric disturbance magnetic field continuation from the ground to the ionosphere using spherical elementary current systems: Earth, Planets and Space, v. 51, no. 6, p. 431–440.

Bonnevier, B., Boström, R., and Rostoker, G., 1970, A three-dimensional model current system for polar magnetic substorms: Journal of Geophysical Research, v. 75, no. 1, p. 107–122.

Boström, R., 1964, A model of the auroral electrojets: Journal of Geophysical Research, v. 69, no. 23, p. 4983–4999.

Boteler, D.H., 2001, Space weather effects on power systems: Washington D.C., American Geophysical Union Geophysical Monograph Series, v. 125, p. 347–352.

Buchanan, A., Finn, C., Love, J.J., Worthington, E.W., Lawson, F., Maus, S., Okewunmi, S., and Poedjono, B., 2013, Geomagnetic referencing—The real-time compass for directional drillers: Oilfield Review, v. 25, no. 3, p. 32–47.

Chapman, S., and Bartells, J., 1940, Spherical harmonic analysis in geophysics: Oxford, England, Oxford University Press, 606 p.

Constable, C., 2007, Geomagnetic spectrum, temporal, *in* Gubbins, D., and Herrero-Bervera, E., eds., Encyclopedia of geomagnetism and paleomagnetism: Dordrecht, Springer, p. 353–355.

Fiori, R.A.D., 2020, Spherical cap harmonic analysis techniques for mapping high-latitude ionospheric plasma flow—Application to the swarm satellite mission, *in* Dunlop, M., and Lühr, H., eds., Ionospheric multi-spacecraft analysis tools: Cham, Springer International Publishing, ISSI Scientific Report Series, v. 17, p. 189–218.

Fukushima, N., 1976, Generalized theorem for no ground magnetic effect of vertical currents connected with Pedersen currents in the uniform-conductivity ionosphere: Report of Ionosphere and Space Research in Japan, v. 30, no. 1/2, p. 35–40.

Haines, G.V., 1985, Spherical cap harmonic analysis: Journal of Geophysical Research, v. 90, no. B3, p. 2583–2591.

Haines, G.V., 1988, Computer programs for spherical cap harmonic analysis of potential and general fields: Computers & Geosciences, v. 14, no. 4, p. 413–447.

Haines, G.V., and Torta, J.M., 1994, Determination of equivalent current sources from spherical cap harmonic models of geomagnetic field variations: Geophysical Journal International, v. 118, no. 3, p. 499–514.

Holmes, R.R., Jr., Jones, L.M., Eidenshink, J.C., Godt, J.W., Kirby, S.H., Love, J.J., Neal, C.A., Plant, N.G., Plunkett, M.L., Weaver, C.S., Wein, A., and Perry, S.C., 2013, U.S. Geological Survey natural hazards science strategy—Promoting the safety, security, and economic well-being of the nation: U.S. Geological Survey Circular 1383-F, 79 p.

Kageyama, A., Sugiyama, T., Watanabe, K., and Sato, T., 2006, A note on the dipole coordinates: Computers & Geosciences, v. 32, no. 2, p. 265–269.

Kelbert, A., Meqbel, N., Egbert, G.D., and Tandon, K., 2014, ModEM—A modular system for inversion of electromagnetic geophysical data: Computers & Geosciences, v. 66, p. 40–53.

Kepko, L., McPherron, R.L., Amm, O., Apatenkov, S., Baumjohann, W., Birn, J., Lester, M., Nakamura, R., Pulkkinen, T.I., and Sergeev, V., 2015, Substorm current wedge revisited: Space Science Reviews, v. 190, p. 1–46.

Kisabeth, J.L., and Rostoker, G., 1977, Modelling of three-dimensional current systems associated with magnetic substorms: Geophysical Journal of the Royal Astronomical Society, v. 49, no. 3, p. 655–683.

Love, J.J., Kelbert, A., Murphy, B.S., Rigler, E.J., and Lewis, K.A., 2020, Geomagnetism Program research plan, 2020–2024: U.S. Geological Survey Circular 1469, 19 p., accessed September 10, 2020, at https://doi.org/10.3133/cir1469.

Love, J.J., and Rigler, E.J., 2014, The magnetic tides of Honolulu: Geophysical Journal International, v. 197, no. 3, p. 1335–1353.

Love, J.J., Rigler, E.J., Pulkkinen, A., and Balch, C.C., 2014, Magnetic storms and induction hazards: Eos, Transactions American Geophysical Union, v. 95, no. 48, p. 445–446.

Lyon, J.G., Fedder, J.A., and Mobarry, C.M., 2004, The Lyon–Fedder–Mobarry (LFM) global MHD magnetospheric simulation code: Journal of Atmospheric and Solar-Terrestrial Physics, v. 66, no. 15–16, p. 1333–1350.

Marsal, S., Torta, J.M., Segarra, A., and Araki, T., 2017, Use of spherical elementary currents to map the polar current systems associated with the geomagnetic sudden commencements on 2013 and 2015 St. Patrick's Day storms: Journal of Geophysical Research, Space Physics, v. 122, no. 1, p. 194–211.

McLay, S.A., and Beggan, C.D., 2010, Interpolation of externally-caused magnetic fields over large sparse arrays using Spherical Elementary Current Systems: Annales Geophysicae, v. 28, no. 9, p. 1795–1805.

McPherron, R.L., Russel, C.T., Kivelson, M.G., and Coleman, P.J., Jr., 1973, Substorms in space—The correlation between ground and satellite observations of the magnetic field: Radio Science, v. 8, no. 11, p. 1059–1076.

Merkin, V.G., and Lyon, J.G., 2010, Effects of the low-latitude ionospheric boundary condition on the global magnetosphere: Journal of Geophysical Research, Space Physics, v. 115, no. A10202, 15 p., accessed October 13, 2011, at https://doi.org/10.1029/2010JA015461.

National Science and Technology Council, 2019, National Space Weather Strategy and Action Plan: Washington, D.C., National Science and Technology Council, 22 p., accessed January 27, 2020, at https://trumpwhitehouse.archives.gov/wp-content/uploads/2019/03/National-Space-Weather-Strategy-and-Action-Plan-2019.pdf.

Pothier, N.M., Weimer, D.R., and Moore, W.B., 2015, Quantitative maps of geomagnetic perturbation vectors during substorm onset and recovery: Journal of Geophysical Research, Space Physics, v. 120, no. 2, p. 1197–1214.

Pulkkinen, A., Amm, O., and Viljanen, A., 2003a, Ionospheric equivalent current distributions determined with the method of spherical elementary current systems: Journal of Geophysical Research, Space Physics, v. 108, no. A21053, 9 p., accessed February 27, 2013, at https://doi.org/10.1029/2001JA005085.

Pulkkinen, A., Amm, O., and Viljanen, A., and BEAR Working Group, 2003b, Separation of the geomagnetic variation field on the ground into external and internal parts using the spherical elementary current system method: Earth, Planets and Space, v. 55, p. 117–129.

Pulkkinen, A., Bernabeu, E., Thomson, A., Viljanen, A., Pirjola, R., Boteler, D., Eichner, J., Cilliers, P.J., Welling, D., Savani, N.P., Weigel, R.S., Love, J.J., Balch, C., Ngwira, C.M., Crowley, G., Schultz, A., Kataoka, R., Anderson, B., Fugate, D., Simpson, J.J., and MacAlester, M., 2017, Geomagnetically induced currents—Science, engineering, and applications readiness: Space Weather, v. 15, no. 7, p. 828–856.

Raeder, J., McPherron, R.L., Frank, L.A., Kokubun, S., Lu, G., Mukai, T., Paterson, W.R., Sigwarth, J.B., Singer, H.J., and Slavin, J.A., 2001, Global simulation of the geospace environment modeling substorm challenge event: Journal of Geophysical Research, Space Physics, v. 106, no. A1, p. 381–395.

Raeder, J., Wang, Y., and Fuller-Rowell, T.J., 2013, Geomagnetic storm simulation with a coupled magnetosphere-ionosphere-thermosphere model, *in* Song, P., Singer, H.J., and Siscoe, G.L., eds., Geophysical Monograph Series: Washington, D.C., American Geophysical Union, v. 125, p. 377–384.

Rastätter, L., Tóth, G., Kuznetsova, M.M., and Pulkkinen, A.A., 2014, CalcDeltaB—An efficient postprocessing tool to calculate ground-level magnetic perturbations from global magnetosphere simulations: Space Weather, v. 12, no. 9, p. 553–565.

Rigler, E.J., Fiori, R.A.D., Pulkkinen, A.A., Wiltberger, M., and Balch, C., 2019, Interpolating geomagnetic observations—Techniques and comparisons, chap. 2 *of* Gannon, J.L., Swidinski, A., and Xu, Z., eds., Geomagnetically induced currents from the sun to the power grid: American Geophysical Union, p. 15–41.

Swisdak, M., 2006, Notes on the dipole coordinate system: Cornell University, Space Physics, arXiv:physics/0606044, 6 p.

Tóth, G., Sokolov, I.V., Gombosi, T.I., Chesney, D.R., Clauer, C.R., De Zeeuw, D.L., Hansen, K.C., Kane, K.J., Manchester, W.B., Oehmke, R.C., Powell, K.G., Ridley, A.J., Roussev, I.I., Stout, Q.F., Volberg, O., Wolf, R.A., Sazykin, S., Chan, A., Yu, B., and Kóta, J., 2005, Space weather modeling framework—A new tool for the space science community: Journal of Geophysical Research, v. 110, no. A12, article no. A12226.

Tsurutani, B.T., Gonzalez, W.D., Kamide, Y., and Arballo, J.K., eds., 1997, Magnetic storms: Washington, D.C., American Geophysical Union, Geophysical Monograph Series v. 98, 266 p.

Vanhamäki, H., and Juusola, L., 2018, Review of data analysis techniques for estimating ionospheric currents based on MIRACLE and satellite observations, *in* Kelling, A., Marghitu, O., and Wheatland, M., eds., Electric currents in geospace and beyond: American Geophysical Union, p. 407–426.

Vanhamäki, H., and Juusola, L., 2020, Introduction to spherical elementary current systems, *in* Dunlop, M.W., and Lühr, H., eds., Ionospheric multi-spacecraft analysis tools: Springer International Publishing, Cham, p. 5–33.

Vanhamäki, H., Maute, A., Alken, P., and Liu, H., 2020, Dipolar elementary current systems for ionospheric current reconstruction at low and middle latitudes: Earth, Planets and Space, v. 72, article no 146, 14 p., accessed October 15, 2020, at https://doi.org/10.1186/s40623-020-01284-1.

Wardinski, I., 2007, Geomagnetic secular variation, *in* Gubbins, D., and Herrero-Bervera, E., eds., Encyclopedia of geomagnetism and paleomagnetism: Dordrecht, Springer Netherlands, p. 346–350.

Waters, C.L., Gjerloev, J.W., Dupont, M., and Barnes, R.J., 2015, Global maps of ground magnetometer data: Journal of Geophysical Research, Space Physics, v. 120, no. 11, p. 9651–9660.

Wei, L.H., Homeier, N., and Gannon, J.L., 2013, Surface electric fields for North America during historical geomagnetic storms: Space Weather, v. 11, no. 8, p. 451–462.

Weimer, D.R., 2005, Improved ionospheric electrodynamic models and application to calculating Joule heating rates: Journal of Geophysical Research, Space Physics, v. 110, no. A5, article no. A05306, 21 p., accessed October 13, 2011, at https://doi.org/10.1029/2004JA010884.

Weygand, J.M., Amm, O., Viljanen, A., Angelopoulos, V., Murr, D., Engebretson, M.J., Gleisner, H., and Mann, I., 2011, Application and validation of the spherical elementary currents systems technique for deriving ionospheric equivalent currents with the North American and Greenland ground magnetometer arrays: Journal of Geophysical Research, Space Physics, v. 116, no. A3, article no. A03305, 8 p., accessed January 17, 2013, at https://doi.org/10.1029/2010JA016177.

Weygand, J.M., and Wing, S., 2016, Comparison of DMSP and SECS region-1 and region-2 ionospheric current boundary: Journal of Atmospheric and Solar-Terrestrial Physics, v. 143–144, p. 8–13.

Xu, Z., Gannon, J.L., and Rigler, E.J., 2013, Report of geomagnetic pulsation indices for space weather applications: U.S. Geological Survey Open-File Report 2013–1166, 22 p., accessed September 11, 2013, at https://doi.org/10.3133/ofr20131166.

Yu, Y., Ridley, A.J., Welling, D.T., and Tóth, G., 2010, Including gap region field-aligned currents and magnetospheric currents in the MHD calculation of ground-based magnetic field perturbations: Journal of Geophysical Research, Space Physics, v. 115, no. A8, article no. A08207, 11 p., accessed October 12, 2020, at https://doi.org/10.1029/2009JA014869.

Appendix 1. Algorithms

The appendix contains mathematical pseudo code that describes algorithms referenced in the main text. This is a mix of formal mathematical notation, and notation common to many computer programming languages (for example, “+“ is addition, “*” is multiplication, “**” is exponentiation).

Algorithms 1, 2, and 3 are available at https://doi.org/10.3133/sir20215123.

Algorithm 1. Pseudocode to Generate Type 1 DALEC in Spherical Coordinates

Algorithm 2. Pseudocode to Generate Type 2 DALEC in Spherical Coordinates

Algorithm 3. Pseudocode for Biot-Savart Integration in Cartesian Coordinates

ISSN 2328-0328 (online)
https://doi.org/10.3133/sir20215123